

# Learning Feedforward and Recurrent Deterministic Spiking Neuron Network Feedback Controllers

**Tae Seung Kang<sup>1</sup> and Arunava Banerjee<sup>1</sup>**

<sup>1</sup>Computer and Information Science and Engineering Department, University of Florida.

**Keywords:** Spiking neuron network, feedback control

## Abstract

We address the problem of learning feedback control where the controller is a network constructed solely of deterministic spiking neurons. In contrast to previous investigations that were based on a spike rate model of the neuron, the control signal here is determined by the precise temporal positions of spikes generated by the output neurons of the network. We model the problem formally as a hybrid dynamical system comprised of a closed loop between a plant and a spiking neuron network. We derive a novel synaptic weight update rule via which the spiking neuron network controller learns to hold process variables at desired set points. The controller achieves its learn-

ing objective based solely on access to the plant’s process variables and their derivatives with respect to changing control signals; in particular, it requires no internal model of the plant. We demonstrate the efficacy of the rule by applying it to the classical control problem of the cart-pole (inverted pendulum) and a model of fish locomotion. Experiments show that the proposed controller has a stability region comparable to a traditional PID controller, its trajectories differ qualitatively from those of a PID controller, and in many instances the controller achieves its objective using very sparse spike train outputs.

## 1 Introduction

Animals are exquisite control systems. Whether it be the flight of a dragonfly or the walking of a biped, state-of-the-art engineered systems are yet to achieve the versatility and robustness displayed by their animal counterparts. In addition, in many instances the particular control task, locomotion for instance, is *learned* by the animal. Our goal in this work is to address this question of learning to control in the context of a biologically motivated constraint—the fact that the vast majority of neurons in animal brains communicate with one another using action potentials, also known as spikes.

In higher animals, several neural sub-systems interact synergistically to achieve the overall control objective. In vertebrates, for example, the control signals received by the effector skeletal muscle fibres are in the form of spike trains generated by lower motor neurons [26]. The controller itself is a network of spiking neurons that resides upstream from the lower motor neurons, hypothesized to be located in the basal ganglia

and the cerebellum [26]. The controller receives inputs, which in the case of a feedback controller are process variables that are to be maintained at fixed or dynamically varying set points. The process variable input into the controller is in turn computed elsewhere and incorporates the combined and integrated output of one or more sensory systems as well as the output of the muscle spindles.

To formally delineate the problem of learning a spiking neuron network controller, we abstract away all aspects of the system that are of secondary concern and replace them with fixed predefined modules. In particular, we model the entire process beginning at the spike train output of the controller and culminating at the control signal generated (such as the force exerted by the muscle fibres) using fixed functions of the spike train. Although our framework can accommodate any deterministic, differentiable mapping from a bounded time window of the spike train output of the controller to a continuous time control signal, for the sake of clarity, we focus on functions that are additively separable. In effect, the continuous time control signal is generated by convolving the spike train output of the controller with fixed causal differentiable kernels of bounded support.

The impact of the control signal on the organism immersed in its environment, we model using a fixed plant. Finally, we model the input of the process variables and their dynamically varying set points as postsynaptic potential inputs into specifically identified neurons of the controller. Our objective is to devise a formal synaptic weight update rule that when applied to the neurons of the controller, induces the controller to learn to perform the control task. We have confined ourselves to a framework where the controller is allowed access solely to derivatives of the plant's process variables with

respect to changing control signals, to achieve its learning objective. In particular, the controller does not have access to any internal forward model of the plant.

That the above problem differs from those previously studied in feedback control, can be discerned from the following observation. Traditional feedback controllers such as the proportional-integral-derivative (PID) controller or its variants are designed to solve a control problem in the continuous domain with few restrictions. The process variable is a bounded continuous function of time, and so is the control signal generated by the controller; there is little else that constrains these functions. In contrast, the control output generated by the spiking neuron network controller is an ensemble of spike trains. The spike trains when convolved with the fixed convolution kernels referred to above, lead to a highly restricted and stereotyped signal. In particular, it is easy to observe that given a kernel, there exists a bound  $C$  such that any non-zero control signal  $u$  satisfies  $\|u\|_\infty > C$ —informally, the controller has the choice between generating no output or an output larger than a fixed amplitude. This has immediate implications for the stability of the fixed point (determined by the set point) of the combined (the controller and the plant in closed loop) dynamical system; the process variable can at best be made to oscillate around the set point.

Finally, we emphasize that the present work considers a controller that lacks an explicit internal model [14] of the plant. How an internal model may represent the putative future state of the plant using spike trains, and how such an internal model may be learned, are complex problems in their own right that are outside the scope of this article.

The remainder of the paper is structured as follows. Following a review of related

work in Section 2, we formally define the coupled dynamical system framework in Section 3. We highlight the difficulty facing analysis when operating with both continuous time signals as well as spike times in the same model, and delineate the approach that resolves this issue. Section 4 then describes the neuron model, and Section 5 briefly describes the two plants investigated in this work, noting their process variables and corresponding set points. Section 6 comprises the core of our contribution where the synaptic weight update rule is derived. Sections 7, 8, and 9 present experimental results from several variations of the controller, and Section 10 concludes with final remarks.

## **2 Background**

Animal motor control investigated through the lens of control theory has a long and rich history. Early theories aiming to explain why coordinated movement in animals was stereotypical in spite of the existence of redundant biomechanical degrees of freedom, appealed to inherent constraints imposed by the nervous system as well as synergies in muscle groups [9, 10, 28, 30]. These theories have since been supplanted by what is now the dominant viewpoint in the field advanced by optimal control theory. This view posits that coordinated movement and trajectory planning can be formally posed as an optimization problem on a cost function that not only accounts for the final goal of the intended activity, but also penalizes path integrated considerations such as total squared jerk [11, 21, 31] or sum of squared motor commands [33]. A variation of optimal control theory, optimal feedback control theory [29], incorporates instantaneous sensory feedback into this framework. The primary goal of these theories is to elucidate

the nature of the control policies and they, therefore, do not address how such control policies may have come to be implemented in neuronal hardware.

In a largely independent strand of research, substantial strides have been made in recent years in learning in feedforward networks of spiking neurons. One of the early results was that of the *SpikeProp* supervised learning rule [7] where a feedforward network of spiking neurons was trained to generate a desired pattern of spikes in the output neurons in response to an input spike pattern of bounded length, with the caveat that each output neuron spike exactly once in the prescribed time window during which the network received the input. Posing the problem differently, [18] proposed the *Tempotron* that learned to discriminate between two sets of bounded length input spike trains by generating an output spike in the first case and remaining quiescent in the second. Subsequent results [4, 13, 23, 24] have relaxed most constraints to the extent that one can now learn precise spike train to spike train transformations in feedforward networks of spiking neurons via a general synaptic weight update rule.

Thus far, attempts to model controllers using spiking neuron networks have used a spike rate based coding of the underlying continuous time signals. For example, [8] have proposed a spiking neuron network based controller that learns using spike time dependent plasticity [25]. The controller displays high firing rates due to the underlying rate based code. Elsewhere, genetic algorithms have been used to construct such controllers, again within the rate code paradigm [6, 12, 19, 27, 32]. Finally, [15, 20] have studied control problems under the framework of reinforcement learning, where the actor-critic model [1, 5] is used to train the networks.

The synaptic weight update rule that is derived in this article generalizes the model

presented in [4] to recurrent networks and, furthermore, incorporates into the framework neurons that not only receive spike input but also continuous time postsynaptic potential inputs representing the process variables and their dynamically varying set points. The feedback control problem is then turned into a learning problem where the objective is for the controller to learn synaptic weights so as to be able to hold process variables at prescribed set points. Theoretical and experimental results restricted to feedforward networks were presented in [22].

### 3 Framework

Our objective is described schematically in Figure 1. We consider a hybrid dynamical system comprised of a closed loop between a plant and a network of spiking neurons that models the controller. The plant is, in general, governed by a non-linear differential equation,  $\dot{x} = f(x, u, t)$  where  $x(t)$  and  $u(t)$  are the vector valued process and control variables, respectively. We consider the scenario where the controller does not have an explicit internal model of  $f(\cdot)$ . The objective of the controller is merely to hold the process variable  $x(t)$  as close as possible to the set point  $x^*(t)$  by generating a control signal  $u(t)$ . The set point  $x^*(t)$  may have been computed by a forward model present elsewhere in the system. Furthermore, our framework is agnostic to whether the trajectory  $x^*(t)$  is precomputed, or is computed on-line based on the current state of the plant.

All neurons in the controller network generate spikes as output, deterministically, according to a minor variation of a standard neuron model that we describe in Section 4.

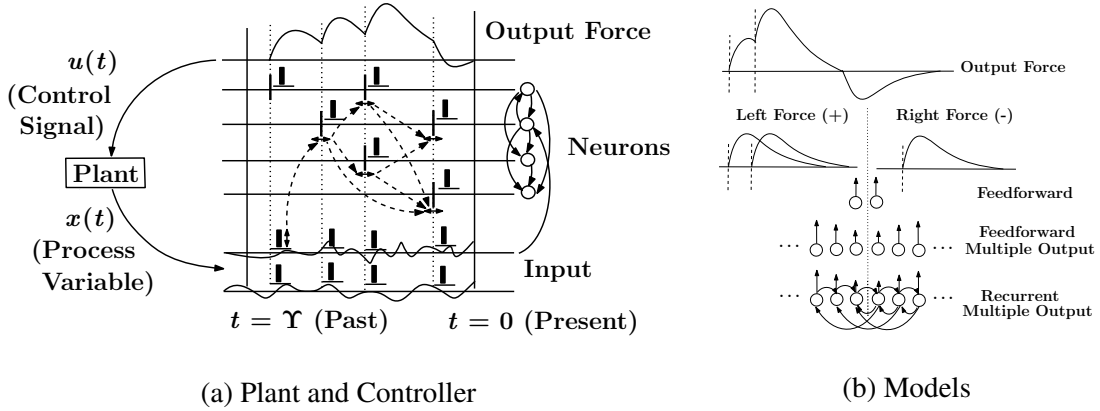


Figure 1: (a) The hybrid dynamical system that models the control problem. The plant receives control input  $u(t)$  and outputs process variable  $x(t)$  according to  $\dot{x} = f(x, u, t)$ . The controller is a feedforward or recurrent network of spiking neurons that takes as input  $x(t)$  and generates output spike trains, which are then convolved with fixed kernels to produce  $u(t)$ . Horizontal lines with arrows represent perturbations in spike times. Vertical bars represent weights assigned to spikes, or in the case of continuous time signals, to weights assigned to temporal segments of the signal. Dotted arrows indicate how perturbations in weights perturb spike times of future spikes generated in the network. Perturbing the synaptic weights of any neurons in the network, in the past, perturbs the output spike times of the output neurons in the network, which when convolved with the kernel creates a perturbation in the control signal. The controller is optimized based on an error function that embodies the deviation of the process signal from its set point. (b) Models. We consider three models: Feedforward network with single kernel, Feedforward network with multiple kernels, and recurrent network with multiple kernels.

The input neurons of the controller receive the continuous time  $x(t)$  (and  $x^*(t)$  in the case of a time varying set point) as postsynaptic potentials in addition to postsynaptic potentials induced by spikes received from other neurons in the network. That the behavior of a putative controller would be different from a standard feedback controller follows immediately from the following observation. Assuming finite non-zero thresholds for all neurons in the network and a simple scenario of  $x^*(t) = 0$ , it is clear that the input neurons will not generate any spikes for sufficiently small  $x(t)$ , and therefore the controller cannot react to deviations away from the set point that are below a sensitivity threshold.

Each output neuron of the controller generates spike trains that are then mapped to a control signal  $u(t)$  via a deterministic function  $\kappa(t_1^O, t_2^O, \dots)$ , where  $t_i^O$  is the  $i$ th output spike time of the output neuron. By convention,  $t_i^O$  is a positive real number denoting the time that has elapsed since the generation of spike  $i$ . Although our framework seamlessly generalizes to any differentiable function with bounded support, for the sake of clarity we consider an additively separable differentiable function with bounded support, that is,  $u(t) = \sum_i \kappa(t_i^O)$  where  $\kappa(t) = 0$  for  $t < 0$  and  $t > \Upsilon$ . If the spikes were to be modeled as Dirac delta functions, this could alternatively be viewed as convolving the spike train with a fixed causal kernel of bounded support. Once again the difference in behavior of a putative controller is clear from the observation that not only is  $u(t)$  highly stereotyped, but there also exists a bound  $C$  such that any non-zero control signal  $u$  satisfies  $\|u\|_\infty > C$ .

The controller network is parameterized by the set of synaptic weights of all synapses in the network. Our overall goal is to demonstrate that these synaptic weights can be

*learned*. Our approach is based on identifying whether small perturbations in the synaptic weights in the past could have led to a slightly superior control signal at present. Superior is objectivized by determining whether the process variable  $x(t)$  would then have been closer to the control point  $x^*(t)$  at the current time  $t = 0$ . The network is then trained using stochastic gradient descent on this objective. Since as noted earlier, the network has an intrinsic sensitivity threshold, the stopping criterion for learning is based on this threshold.

The primary difficulty in the problem arises from the need to model continuous time signals such as  $x(t)$  or  $u(t)$  and spike times of the neurons in the network, under a common framework. To resolve this problem we negotiate several refinements. First, we approach the problem via a perturbation analysis. Whereas the continuous time signals are perturbed in the range, as is standard, spikes, on the other hand, are set as stereotyped objects that can only be perturbed in time (indicated by horizontal arrows in Figure 1a). Second, we assume that the neurons in the network are bounded memory devices; the effect of a past spike on the current membrane potential of a neuron is 0 if the spike has aged beyond a time bound  $\Upsilon$ . Noting that neurons have an absolute refractory period that prevents successive spikes from occurring closer than a certain time bound, we can conclude that there can only be finitely many spikes in the window  $[0, \Upsilon]$  that have an impact on the current membrane potentials of the neurons in the network. The perturbation analysis, consequently, is confined to finitely many spikes in the past. Third, noting that any learning algorithm updates synaptic weights, successive spikes arriving at the same synapse can have different effects on the postsynaptic potential of the neuron. We accommodate this in the analysis by virtually assigning synaptic

weights to spikes rather than to the synapse (indicated by vertical bars in Figure 1a). Likewise, for the continuous time signals, we assign synaptic weights to segments of the signal in the past. Fourth, we restrict synaptic weight updates to those instants in time where spikes are generated by the output neurons of the network. Finally, noting that the effects of spikes as well as of the continuous signals are causal on other spikes generated in the network (indicated by the dotted arrows in Figure 1a), we surmise that regardless of the network architecture, whether it be feedforward or recurrent, the effect of perturbations form a partial order in time. Brought together, these refinements result in a well defined synaptic weight update rule as is demonstrated in upcoming sections.

We probe three model architectures of successively increasing complexity, based on connectivity and the number of output neurons in the controller network and their corresponding  $\kappa(\cdot)$  functions (Figure 1b). Model 1, the simplest model, is defined as a network with the simplest possible architecture, that is no hidden layers. In order to model a  $u(t)$  whose value can be positive or negative, we use two output neurons with positive valued  $\kappa(\cdot)$  and set  $u(t)$  to be their difference. Model 2, the model of intermediate complexity, is defined as a network with four or more output neurons (groups of two or more) with distinct  $\kappa(\cdot)$ 's, with a feedforward architecture comprised of one or more hidden layers. Model 3, the most general model, is defined as a recurrent network where the output neurons are fully connected with each other as well as other neurons in the network. The synaptic weight update rule that we derive is general and applies to all architectures.

## 4 Neuron Model

We use a minor variation of the Spike Response Model [17] for the neurons in our controller. The membrane potential of a neuron is computed as the sum of postsynaptic potentials elicited by spikes arriving at its various synapses from other neurons in the network, and afterhyperpolarization potentials elicited by the spikes generated by the neuron itself. A special class of neurons, the input neurons, have process variables directly injected as additional postsynaptic potentials. We assume in addition that all afferent (incoming) and efferent (outgoing) spikes that were generated earlier than  $t = \Upsilon$  in the past have no effect on the present membrane potential of the neuron (See Figure 1a). The neuron generates a spike when the membrane potential crosses the threshold  $\Theta$  from below.

The postsynaptic potential elicited by a spike is computed as the product of the synaptic weight at the time of the arrival of the spike at the synapse with the prototypical postsynaptic response function assigned to that synapse. Likewise, the postsynaptic potential elicited by the continuous time process variable is computed as the product of the synaptic weight at the current time with the current value of the process variable. Since the learning algorithm updates all synaptic weights whenever spikes are generated by the output neurons of the controller, to enable the analysis of the system over any finite stretch of time, past synaptic weights are virtually assigned to the corresponding spikes in the case of synapses that receive spikes, and to the corresponding intervals of time in the case of synapses receiving continuous time process variable inputs. Finally, each spike generated by the neuron elicits a prototypical afterhyperpolarization potential. The present is set at  $t = 0$  with  $t > 0$  denoting the past.

Formally, the membrane potential,  $P$  of a neuron at the present time  $t = 0$  is given by

$$P = \sum_{i \in \Gamma_c} \tilde{w}_{i,0} x_i(0) + \sum_{i \in \Gamma_s} \sum_{j \in \mathcal{F}_i} w_{i,j} \xi(t_{i,j}^I) + \sum_{k \in \mathcal{F}} \eta(t_k^O). \quad (1)$$

where  $\Gamma_c$  is the set of synapses receiving the continuous time process variable inputs,  $\Gamma_s$  is the set of synapses receiving afferent spikes from other neurons in the network,  $\mathcal{F}_i$  is the set of previous spikes that have arrived at synapse  $i$ , and  $\mathcal{F}$  is the set of previous spikes generated by the neuron.  $\tilde{w}_{i,0}$  is the weight of continuous time input synapse  $i$  immediately after the most recent output spike of the system, and therefore in general,  $\tilde{w}_{i,l}$  is the synaptic weight over the interval between the  $l$ th and  $(l + 1)$ th most recent output spike of the system. Since synaptic weights are updated at the times of generation of spikes at the output neurons of the controller, it follows that  $\tilde{w}_{i,0}$  is the current weight of synapse  $i$ .  $w_{i,j}$  is the weight of the  $j$ th most recent afferent spike at synapse  $i$  receiving spike input.  $\xi(\cdot)$  is the prototypical postsynaptic potential elicited by an afferent spike and  $\eta(\cdot)$  is the prototypical afterhyperpolarization potential elicited by an efferent spike.  $t_{i,j}^I$  is the time elapsed since the arrival of the  $j$ th most recent spike at synapse  $i$ , and  $t_k^O$  is the time since the generation of the  $k$ th most recent efferent spike.

The functional form of  $\xi(\cdot)$  that we have used (and this can be modified without affecting the analysis) is

$$\xi(t) = \frac{e^{-\beta d^2/t}}{d\sqrt{t}} e^{-t/\tau} \quad \text{for } 0 < t \leq \Upsilon \quad \text{and } 0 \text{ otherwise} \quad (2)$$

where  $\beta$  and  $\tau$  control the rate of rise and fall of the postsynaptic potential, and  $d$

denotes the distance of the synapse from the soma. Likewise, the functional form of  $\eta(\cdot)$  is

$$\eta(t) = Re^{-t/\gamma} \quad \text{for } 0 < t \leq \Upsilon \quad \text{and } 0 \text{ otherwise} \quad (3)$$

where  $R$  denotes the instantaneous fall in potential after a spike and  $\gamma$  controls its rate of recovery.

## 5 Overview of Plants

### 5.1 Inverted Pendulum

The first plant we consider in this article is the classical control problem of the cart-pole (also known as the inverted pendulum) as shown in Figure 2a. The cart-pole comprises of an inverted rigid pendulum, with the mass at the top. The pendulum is fulcrumed at its base to the cart which rests on a frictionless surface. Control signals mapped to forces can be applied to the cart to move it along the horizontal axis. The control problem is to apply forces to the cart to maintain the upright position of the pendulum. The process variables that we have considered for this plant are:  $\theta$ , the angular deviation of the pendulum from the upright position, and  $\dot{\theta}$ , the angular velocity of the pendulum. The set points for the process variables are  $\theta = 0, \dot{\theta} = 0$ . The details of the system dynamics can be found in [1]. All quantities of interest as presented in Section 6, we have derived through numerical computations.

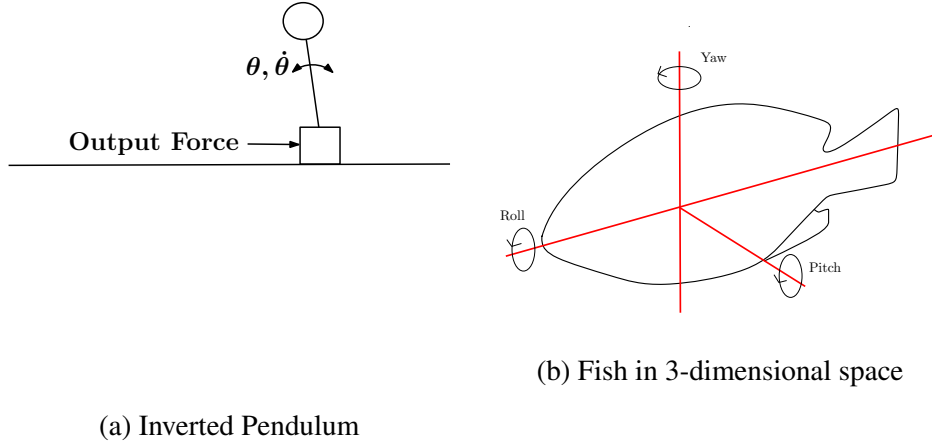


Figure 2: (a) Inverted Pendulum and (b) Fish in 3-dimensional space.

## 5.2 Fish Locomotion

We also consider a more complex plant where a fish swims in 3-dimensional space  $(x, y, z)$  as depicted in Figure 2b. The trajectory of the fish’s center of gravity (*cog*) can be controlled by regulating three time varying control variables, the *yaw*, *pitch*, and *roll*. This control problem is substantially more complex since the control variables have to be regulated in a “synergistic” fashion—the yaw, pitch and roll have to interact to achieve even the simplest of locomotion tasks. The process variables consist of the 3-dimensional coordinate  $(x, y, z)$  of the fish’s *cog* and its orientation  $(\theta_x, \theta_y, \theta_z)$  with respect to a target location. The orientation angles range between  $-180$  and  $180$  degrees with  $(\theta_x, \theta_y, \theta_z) = (0, 0, 0)$  corresponding to the fish facing the target. The target location is given by  $(x^*, y^*, z^*)$ . We have considered a scenario where the set point is fixed at a different  $(x^*, y^*, z^*)$  in each experiment. The fish begins at the origin  $(0, 0, 0)$  and is required to arrive at the target  $(x^*, y^*, z^*)$  using a fixed velocity profile that ramps up from 0, stays constant, and then ramps down to 0.

We have considered several variations of the problem where one or more of the con-

trol variables are shut off and the target  $(x^*, y^*, z^*)$  is set such that the task is achievable using the smaller set of controls. The details of the system dynamics can be found in the SOEIL project [16]. Once again, all quantities of interest as presented in Section 6, we have derived through numerical computations.

## 6 Feedback Control using Spiking Neuron Networks

We now derive a synaptic weight update rule that applies to any connectivity architecture, be it recurrent or feedforward. The basic insight is to focus on the inputs to the neurons, spikes or continuous time, rather than the neurons themselves, and subsequently to realize that regardless of the architecture of the network, the spikes and continuous time inputs arrange themselves in a *causal* partial order (the dotted arrows in Figure 1a). In essence, perturbations to the timing or the weight of a spike, or to the weight assigned to a segment of the continuous time input, cause perturbations in the timing of spikes that are generated at a later time, and therefore, there are no cycles that can invalidate the application of the chain rule.

The graph structure of the impact of perturbations can, however, be very complex, with a spike perturbation causing a perturbation in another spike via various intersecting causal paths. Rather than enumerate all such paths, we resolve this using a recursive/dynamic programming approach, where all effects are computed and stored at the time of generation of each spike in the network. Not only does this approach circumvent the issue of identifying the potentially exponentially many paths, it also fits well with the online nature of the updates.

## 6.1 The error function and control output

The proposed spiking neuron network controller depicted in Figure 1 can be formally modeled as follows. Consider a plant with the current value of the process variables represented by vector  $\langle x_1(0), x_2(0), \dots, x_{\mathcal{D}}(0) \rangle$ , where  $\mathcal{D}$  is the number of process variables to be controlled. The desired state of the plant (i.e., the set point of the process variables) is represented by  $\langle x_1^*(0), x_2^*(0), \dots, x_{\mathcal{D}}^*(0) \rangle$ . The instantaneous error  $E$  can then be defined as  $\frac{1}{2} \sum_{i=1}^{\mathcal{D}} (x_i(0) - x_i^*(0))^2$ . The synaptic update rule that we derive next is based on minimizing this objective using stochastic gradient descent.

A traditional controller receives continuous time process variables from the plant and generates a continuous time control output. The proposed controller, however, generates spike trains, one for each neuron, instead of a continuous output. The spike train generated by each output neuron  $j$  is convolved with the kernel

$$\kappa(t) = te^{-t/\tau_f} \quad \text{for } 0 < t \leq \Upsilon \quad \text{and } 0 \text{ otherwise} \quad (4)$$

to generate a continuous time control output (which we shall henceforth refer to as force due to the nature of the plants we have considered in this article):

$$F_j = \mu_j \sum_{i \in \mathcal{F}_j} \kappa({}^j t_i^O) \quad (5)$$

where  $\tau_f$  is the time constant,  $\mu_j$  is the magnitude assigned to neuron  $j$ ,  ${}^j t_i^O$  is the time elapsed since the generation of the  $i^{\text{th}}$  most recent efferent spike of the output neuron  $j$ , and  $\mathcal{F}_j$  is the set of past spikes of output neuron  $j$ . We observe in passing that we have chosen the above form of the kernel for the sake of simplicity and that our analysis applies to any differentiable kernel function with compact support. The final force  $F$

applied to the plant is

$$F = \sum_j \pm F_j \quad (6)$$

where  $\pm$  represents the sign of  $F_j$ ,  $+$  for neurons with positive forces and  $-$  for those with negative forces (directed opposite to the positive forces). By using groups of neurons with opposing forces, we can set the kernels as positive functions without loss of generality.

## 6.2 Gradient of the error function

Our overall objective is to compute the gradient of the error with respect to the synaptic weights on all the neurons in the controller network. We do this in stages. We first compute the gradient with respect to the output spike times of the output neurons of the controller network. Applying chain rule, we have

$$\frac{\partial E}{\partial(jt_l^O)} = \frac{\partial E}{\partial F} \frac{\partial F}{\partial(jt_l^O)} \quad (7)$$

where  ${}^j t_l^O$  is the time elapsed since the departure of the  $l^{\text{th}}$  most recent efferent spike of output neuron  $j$ , and

$$\frac{\partial E}{\partial F} = \frac{1}{2} \sum_i \frac{\partial(x_i(0) - x_i^*(0))^2}{\partial x_i(0)} \frac{\partial x_i(0)}{\partial F} = \sum_i (x_i(0) - x_i(0)^*) \frac{\partial x_i(0)}{\partial F} \quad (8)$$

and

$$\frac{\partial F}{\partial(jt_l^O)} = \frac{\partial F}{\partial F_j} \frac{\partial F_j}{\partial(jt_l^O)} = \pm \mu_j \left. \frac{\partial \kappa}{\partial t} \right|_{jt_l^O} \quad (9)$$

In Eq (8),  $\frac{\partial x_i(0)}{\partial F}$  is computed as a numerical derivative from the plant:  $\frac{\partial x_i(0)}{\partial F} \approx$

$$\frac{\Delta x_i(0)}{\Delta F}.$$

### 6.3 Perturbation analysis

Our goal now is to determine how perturbations in synaptic weights assigned to spikes or to segments of the continuous time input signal, for any neuron in the controller network, translate to perturbations in the times of the spikes generated by the output neurons of the network. We achieve this by conducting a perturbation analysis across any given individual neuron and combine it with a recursive framework that extends the outcome of the analysis across multiple neurons in the network. A less general analysis that applies to feedforward networks was presented in [22].

We begin by elucidating the notions of a direct effect as opposed to an indirect effect of a perturbation, and in the process construct a recursive framework for the accounting of these effects. Consider any neuron in the network for which the weight or the time of an afferent spike or continuous input at a synapse is perturbed. This perturbation will naturally lead to a perturbation in the time of an output spike that is generated subsequently. What is important to note is that this perturbation of the output spike time is the sum total of two kinds of effects: the first is the direct effect of the perturbation in the input spike, and the second is the indirect effect propagated through the intermediate spikes (the spikes generated in between the input being perturbed and the output spike under consideration) generated by the neuron. To elaborate, a perturbation in the weight or time of an input spike perturbs the immediately generated output spike, which in turn perturbs the time of subsequent output spikes, and so forth. This domino effect, we define as the indirect effect of a perturbation. By definition, then, all perturbations that occur via intermediate spikes, such as across two or more neurons, are indirect effects.

Formally, we identify a direct effect with the partial derivative. So, for example,

$\frac{\partial t_l^O}{\partial w_{i,j}}$  corresponds to the how the time of spike  $t_l^O$  would change if weight  $w_{i,j}$  were perturbed, if all other spike times and weights in the network could be held fixed. In comparison, we identify the total (sum of direct and indirect) effect with the total derivative. So, for example,  $\frac{Dt_l^O}{\partial w_{i,j}}$  corresponds to the how the time of spike  $t_l^O$  would change if weight  $w_{i,j}$  were perturbed, if all perturbations in other spike times and weights in the network due to the change in the weight  $w_{i,j}$  were taken into consideration.

The relationship between the two lends itself naturally to a recursive formulation.

$$\frac{Dt_l^O}{\partial w_{i,j}} = \frac{\partial t_l^O}{\partial w_{i,j}} + \sum_{k \in \Gamma_*} \frac{\partial t_l^O}{\partial t_k^O} \frac{Dt_k^O}{\partial w_{i,j}} \quad (10)$$

where  $\Gamma_*$  is the set of all spikes generated by all neurons in the network since the time of the spike corresponding to  $w_{i,j}$ . The first term corresponds to the direct effect of the weight perturbation and the second term corresponds to the indirect effect through other spikes. Likewise, the total derivative of  $t_l^O$  with respect to the continuous input weight  $\tilde{w}_{i,p}$  is

$$\frac{Dt_l^O}{\partial \tilde{w}_{i,p}} = \frac{\partial t_l^O}{\partial \tilde{w}_{i,p}} + \sum_{k \in \Gamma_*} \frac{\partial t_l^O}{\partial t_k^O} \frac{Dt_k^O}{\partial \tilde{w}_{i,p}} \quad (11)$$

where  $\Gamma_*$  is the set of all spikes generated by all neurons in the network since the segment of continuous input corresponding to  $\tilde{w}_{i,p}$ .

There are only two cases where the direct effect from one spike/ segment of continuous input to another spike is non-zero: input to output across a neuron mediated by the change in postsynaptic potential, and output to output at a neuron mediated by the change in the afterhyperpolarization potential. In all other cases, the direct effect is

zero. We derive the values of these next.

Consider the state of a neuron at the time of the generation of its output spike  $t_l^O$ .

The membrane potential of the neuron is

$$\tilde{\Theta} = \sum_{i \in \Gamma_c} \tilde{w}_{i,l} x_i(t_l^O) + \sum_{i \in \Gamma_s} \sum_{j \in \mathcal{F}_i} w_{i,j} \xi(t_{i,j}^I - t_l^O) + \sum_{k \in \mathcal{F}} \eta(t_k^O - t_l^O). \quad (12)$$

where  $\Gamma_c$  is the set of synapses receiving continuous input,  $\Gamma_s$  is the set of synapses receiving afferent spikes,  $\tilde{w}_{i,l}$  is the weight of synapse  $i$  immediately prior to output spike  $l$ , and  $w_{i,j}$  is the weight of afferent spike  $j$  at synapse  $i$ . Note that we have replaced  $\Theta$  with  $\tilde{\Theta}$  to account for those spikes that at the time of the generation of  $t_l^O$  were less than  $\Upsilon$  old, but are now past that bound. Had the various quantities in Eq (12) been perturbed, we would have

$$\begin{aligned} \tilde{\Theta} &= \sum_{i \in \Gamma_c} (\tilde{w}_{i,l} + \Delta \tilde{w}_{i,l}) x_i(t_l^O + \Delta t_l^O) + \sum_{i \in \Gamma_s} \sum_{j \in \mathcal{F}_i} (w_{i,j} + \Delta w_{i,j}) \xi(t_{i,j}^I + \Delta t_{i,j}^I - t_l^O - \Delta t_l^O) \\ &+ \sum_{k \in \mathcal{F}} \eta(t_k^O + \Delta t_k^O - t_l^O - \Delta t_l^O). \end{aligned} \quad (13)$$

Using a first order Taylor approximation, we get

$$\begin{aligned} \tilde{\Theta} &= \sum_{i \in \Gamma_c} (\tilde{w}_{i,l} + \Delta \tilde{w}_{i,l}) \left( x_i(t_l^O) + \frac{\partial x_i}{\partial t} \Big|_{t_l^O} \Delta t_l^O \right) \\ &+ \sum_{i \in \Gamma_s} \sum_{j \in \mathcal{F}_i} (w_{i,j} + \Delta w_{i,j}) \left( \xi(t_{i,j}^I - t_l^O) + \frac{\partial \xi}{\partial t} \Big|_{(t_{i,j}^I - t_l^O)} (\Delta t_{i,j}^I - \Delta t_l^O) \right) \\ &+ \sum_{k \in \mathcal{F}} \left( \eta(t_k^O - t_l^O) + \frac{\partial \eta}{\partial t} \Big|_{(t_k^O - t_l^O)} (\Delta t_k^O - \Delta t_l^O) \right) \end{aligned} \quad (14)$$

Combining Eq (12) and (14), dropping higher order terms and rearranging, we get

$$\Delta t_l^O = \frac{\sum_{i \in \Gamma_c} \Delta \tilde{w}_{i,l} x_i(t_l^O) + \sum_{i \in \Gamma_s} \sum_{j \in \mathcal{F}_i} \Delta w_{i,j} \xi(t_{i,j}^I - t_l^O) + \sum_{i \in \Gamma_s} \sum_{j \in \mathcal{F}_i} w_{i,j} \frac{\partial \xi}{\partial t} \Big|_{(t_{i,j}^I - t_l^O)} \Delta t_{i,j}^I + \sum_{k \in \mathcal{F}} \frac{\partial \eta}{\partial t} \Big|_{(t_k^O - t_l^O)} \Delta t_k^O}{-\sum_{i \in \Gamma_c} \tilde{w}_{i,l} \frac{\partial x_i}{\partial t} \Big|_{t_l^O} + \sum_{i \in \Gamma_s} \sum_{j \in \mathcal{F}_i} w_{i,j} \frac{\partial \xi}{\partial t} \Big|_{(t_{i,j}^I - t_l^O)} + \sum_{k \in \mathcal{F}} \frac{\partial \eta}{\partial t} \Big|_{(t_k^O - t_l^O)}}. \quad (15)$$

We can now derive the final set of quantities of interest from Eq (15).

$$\frac{\partial t_l^O}{\partial \tilde{w}_{i,l}} = \frac{x_i(t_l^O)}{-\sum_{i \in \Gamma_c} w_{i,l} \frac{\partial x_i}{\partial t} \Big|_{t_l^O} + \sum_{i \in \Gamma_s} \sum_{j \in \mathcal{F}_i} w_{i,j} \frac{\partial \xi}{\partial t} \Big|_{(t_{i,j}^I - t_l^O)} + \sum_{k \in \mathcal{F}} \frac{\partial \eta}{\partial t} \Big|_{(t_k^O - t_l^O)}}, \quad (16)$$

$$\frac{\partial t_l^O}{\partial \tilde{w}_{i,p}} = 0 \quad (p > l), \quad (17)$$

$$\frac{\partial t_l^O}{\partial t_{i,p}^I} = \frac{w_{i,p} \frac{\partial \xi}{\partial t} \Big|_{(t_{i,p}^I - t_l^O)}}{-\sum_{i \in \Gamma_c} w_{i,l} \frac{\partial x_i}{\partial t} \Big|_{t_l^O} + \sum_{i \in \Gamma_s} \sum_{j \in \mathcal{F}_i} w_{i,j} \frac{\partial \xi}{\partial t} \Big|_{(t_{i,j}^I - t_l^O)} + \sum_{k \in \mathcal{F}} \frac{\partial \eta}{\partial t} \Big|_{(t_k^O - t_l^O)}}, \quad (18)$$

$$\frac{\partial t_l^O}{\partial t_p^O} = \frac{\frac{\partial \eta}{\partial t} \Big|_{(t_p^O - t_l^O)}}{-\sum_{i \in \Gamma_c} w_{i,l} \frac{\partial x_i}{\partial t} \Big|_{t_l^O} + \sum_{i \in \Gamma_s} \sum_{j \in \mathcal{F}_i} w_{i,j} \frac{\partial \xi}{\partial t} \Big|_{(t_{i,j}^I - t_l^O)} + \sum_{k \in \mathcal{F}} \frac{\partial \eta}{\partial t} \Big|_{(t_k^O - t_l^O)}}, \quad (19)$$

and

$$\frac{\partial t_l^O}{\partial w_{i,j}} = \frac{\xi(t_{i,j}^I - t_l^O)}{-\sum_{i \in \Gamma_c} w_{i,l} \frac{\partial x_i}{\partial t} \Big|_{t_l^O} + \sum_{i \in \Gamma_s} \sum_{j \in \mathcal{F}_i} w_{i,j} \frac{\partial \xi}{\partial t} \Big|_{(t_{i,j}^I - t_l^O)} + \sum_{k \in \mathcal{F}} \frac{\partial \eta}{\partial t} \Big|_{(t_k^O - t_l^O)}}. \quad (20)$$

## 6.4 Learning rules

Learning is accomplished via gradient descent. As noted earlier, the synaptic weights are updated at the times of the generation of spikes by the output neurons of the network. The reason for this choice is that if there are no such spikes generated, the implication is that the process variables are in a safe range and thus no control signal is necessary. This, in turn, indicates that there is no evidence that necessitates weight changes. Applying chain rule, we get

$$\frac{\partial E}{\partial \tilde{w}_{i,p}} = \sum_{l \in \mathcal{F}} \frac{\partial E}{\partial t_l^O} \frac{Dt_l^O}{\partial \tilde{w}_{i,p}}, \quad (21)$$

and

$$\frac{\partial E}{\partial w_{i,p}} = \sum_{l \in \mathcal{F}} \frac{\partial E}{\partial t_l^O} \frac{Dt_l^O}{\partial w_{i,p}}. \quad (22)$$

These are computed using Eq 7, 10, 11, 16, 17, 18, 19, and 20.

Gradient descent would require

$$w_{i,p} \leftarrow w_{i,p} - \alpha \frac{\partial E}{\partial w_{i,p}} \quad (23)$$

where  $\alpha$  is the learning rate, and likewise for  $\tilde{w}_{i,p}$ . Clearly, however, we can not reach into the past to make these changes. We therefore institute a summed delayed update to the synapse at the current time.

$$w_i \leftarrow w_i - \sum_{p \in \mathcal{F}_i} \alpha \frac{\partial E}{\partial w_{i,p}} \quad (24)$$

and likewise for  $\tilde{w}_i$ .

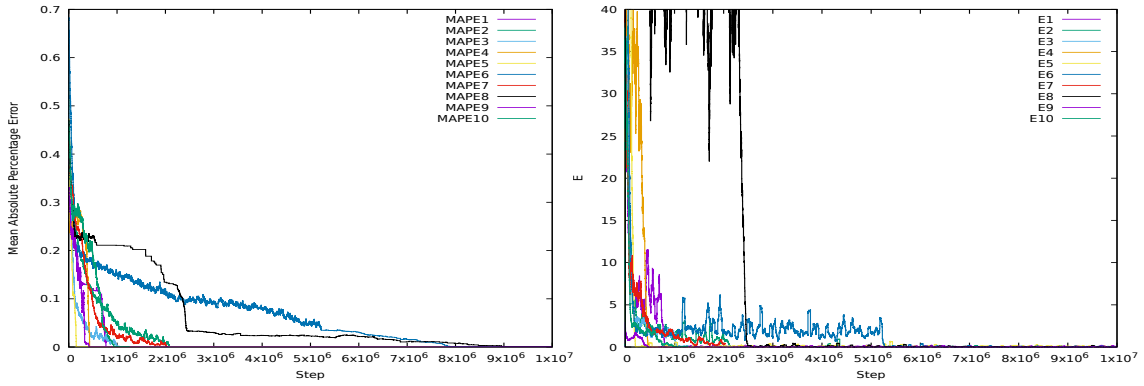
## 7 Experiments - Simulated Data

Recognizing that recurrent networks of spiking neurons can display very complex dynamics [3], we begin by exploring how stochastic gradient descent on synaptic weights influences this behavior. In particular, we explore through simulation experiments three specific questions relevant to the learning problem: (a) does gradient descent converge to the local minima in spite of the complexity of the dynamics of the network, (b) is the energy landscape non-convex, that is, does it have multiple local minimas, and (c) are there multiple network instantiations that can effect the same control behavior?

We addressed these questions in a highly controlled experimental setup where the goal was for a network to learn the input output transformation of a given *putative network* of the same architecture. We considered two neuron recurrent networks with randomly chosen synaptic weights that were driven by a Gaussian process input signal, and whose output spike trains were convolved against kernels that were randomly chosen and fixed. Learning networks with randomly chosen synaptic weights were then trained using the weight update rule presented in the previous section to learn the input output transformation of the putative networks. Progress was measured both in terms of the error,  $E$ , the squared instantaneous difference between the output of the learning versus the putative network, and a far more conservative measure, MAPE<sup>1</sup>, the mean absolute percentage error of the synaptic weights of the learning network with respect to the putative network (with 100% corresponding to 1.0 in the graphs in Figure 3).

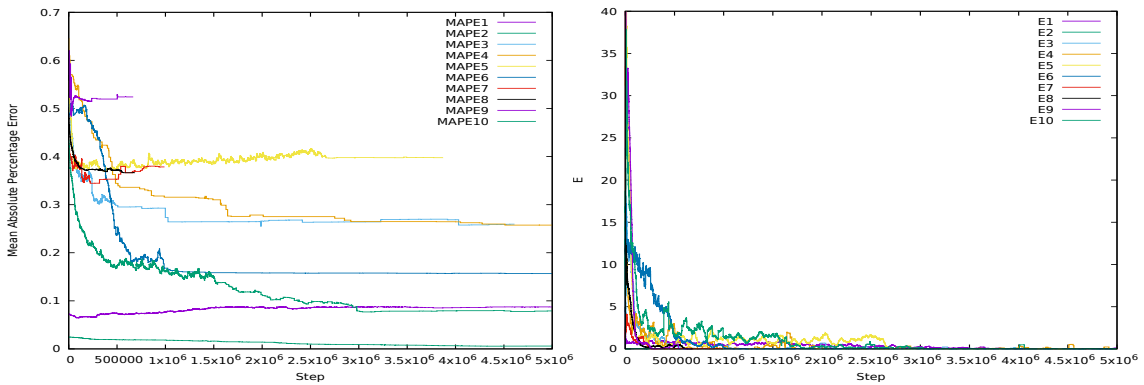
---

<sup>1</sup>The absolute value of the difference between a synaptic weight and the corresponding synaptic weight on the putative network, normalized by the synaptic weight on the putative network, averaged over all synapses in the network.



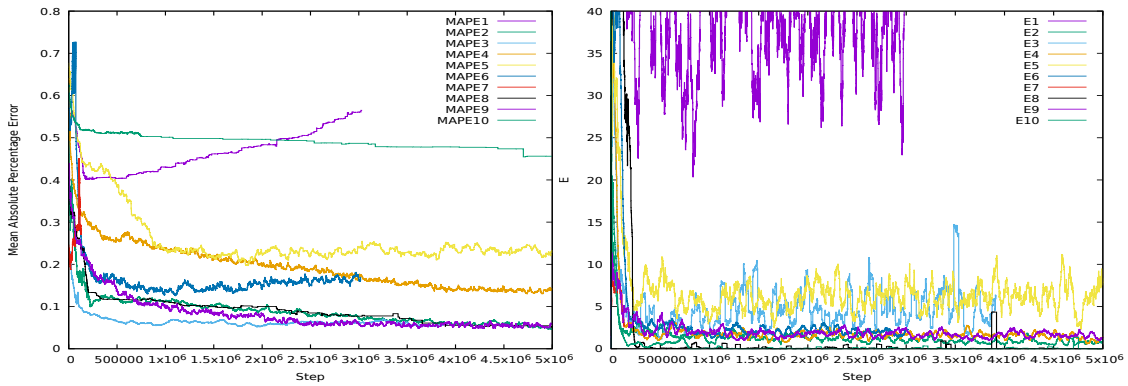
(a) MAPE converges

(b) E converges



(c) MAPE does not converge

(d) E converges



(e) MAPE does not converge

(f) E does not converge

Figure 3: Convergence results for Model 3 (recurrent network) with two output neurons during training. The y-axis for (a), (c) and (e) corresponds to the mean absolute percentage error (MAPE) between the learner's weight vector and the putative network's weight vector. The y-axis for (b), (d), (f) corresponds to the error  $E$ . Captions indicate the kind of behavior observed.

Figure 3, displays the results of a subset of the experiments, grouped by behavior. Each panel shows the learning trajectory of 10 randomly initialized learning networks. The  $x$ -axis corresponds to the number of steps (the stepsize was set to  $1msec$ ), and the  $y$ -axis corresponds to either the MAPE or  $E$ . The convergence criterion was either  $MAPE \leq 0.001$  or  $E \leq 0.001$ , depending on the scenario. The learning rate was set to 0.0001.

Experimental results were grouped under 3 categories depending on the convergence of MAPE and  $E$ : (a) and (b) where both the MAPE and  $E$  converged, (c) and (d) where the MAPE diverged but  $E$  converged, and (e) and (f) where neither the MAPE nor  $E$  converged. As can be observed from the figures, in (a) and (b) most of the MAPEs converged within  $10^7$  steps although some networks took longer. In the case of (c) and (d),  $E$  converged but the MAPE did not, clearly indicating that there are multiple networks that can generate the same output trajectory when driven by identical input. Finally, (e) and (f) correspond to cases where neither the MAPE nor  $E$  converged according to the aforementioned criterion. In Figure 3 (e), MAPE1, MAPE5, and MAPE6 are clearly divergent. The others, although convergent, did not satisfy the criterion in the number of time steps allotted. For MAPE1, MAPE5, and MAPE6, it is clear from the graphs that the learning rate was set too high (the graphs display a standard thrashing behavior).

We conclude that although the  $E$  landscape can have multiple local minimas for a given set of inputs, since multiple networks can generate the same output, it is likely that these networks can learn the necessary control objective over time.

## 8 Experiments - Inverted Pendulum

Next, we experimented with the inverted pendulum, using the code for the plant developed in [2].

### 8.1 Setup

We defined a successful learning event of the controller as having balanced the pole without failure for one hour of simulation time. A failure was defined as an event where the process variables of the pole departed from a certain predefined range. Specifically, the time step for the simulations was set at  $1msec$ , the number of steps for a successful run was set at 3600000 (1 hour), and the predefined range was  $[-0.2094, 0.2094]$  for  $\theta$  and  $[-2.01, 2.01]$  for  $\dot{\theta}$ , respectively. Training of the controller was continued until success. During the training phase, the controller was initialized with random network weights, and the pole was initialized at a random position  $\theta$ , and random angular velocity  $\dot{\theta}$ . The controller network then learned by updating the synaptic weights as defined earlier. If a failure event was triggered as defined above, we restarted the training with random initial weights. Once the network had successfully learned the task, we fixed the weights and tested the controller with random initial plant states to evaluate its robustness.

The plant was configured as: half-pole length  $l = 0.5$  (m), pole mass  $m = 0.1$  (kg), cart mass  $M = 1.0$  (kg), and gravity  $g = 9.8$  ( $m/s^2$ ). The configuration of the controller was: time step =  $1msec$ , threshold = 0.1,  $\beta = 1.0$ ,  $d = 1.5$ ,  $\tau = 20$ ,  $\tau_f = 20$  (msec),  $R = -1000$ ,  $\gamma = 1.2$ , and  $\alpha = 0.01$ . The unit of  $R$  is the same as that of the membrane potential. The magnitude of  $R$  in the afterhyperpolarization was set large

enough to prevent inter spike intervals to fall below  $4 - 5msec$ . We measured the firing rates of the output neurons in Hz (number of spikes per second). In all the experiments, the same PID controller was used for comparison and its parameters were set as  $K_p = 300$ ,  $K_i = 1$ , and  $K_d = 100$ .

## 8.2 Results

We note in passing that when  $\dot{\theta}$  was not provided as an input to the network, the controller failed to learn. However, when the network received both  $\theta$  and  $\dot{\theta}$ , the network learned regardless of whether it was a Model 1, 2 or 3.

### 8.1 Model 1 (Single Kernel Feedforward Network)

The simplest controller network architecture is one where two neurons with force kernels  $+\kappa(t)$  and  $-\kappa(t)$ , respectively, are trained to accomplish the control task. Surprisingly, even in this extremely restricted scenario the network learned the task, although the domain over which the network exercised control was found to be small relative to that of a PID controller. Extensive details of these learning experiments have been presented in [22]. Here we review two aspects that highlight the nature of the resultant controller.

Fig. 4 shows the trajectories of the plant state  $(\theta, \dot{\theta})$  over time with two different initial settings and the coverage over initial states of the controller, both juxtaposed against corresponding behavior of the PID controller. As is clear from the figure, the trajectory of the proposed controller is qualitatively different from that of the PID controller, demonstrating a novel control mechanism. It is also clear that Model 1's coverage is

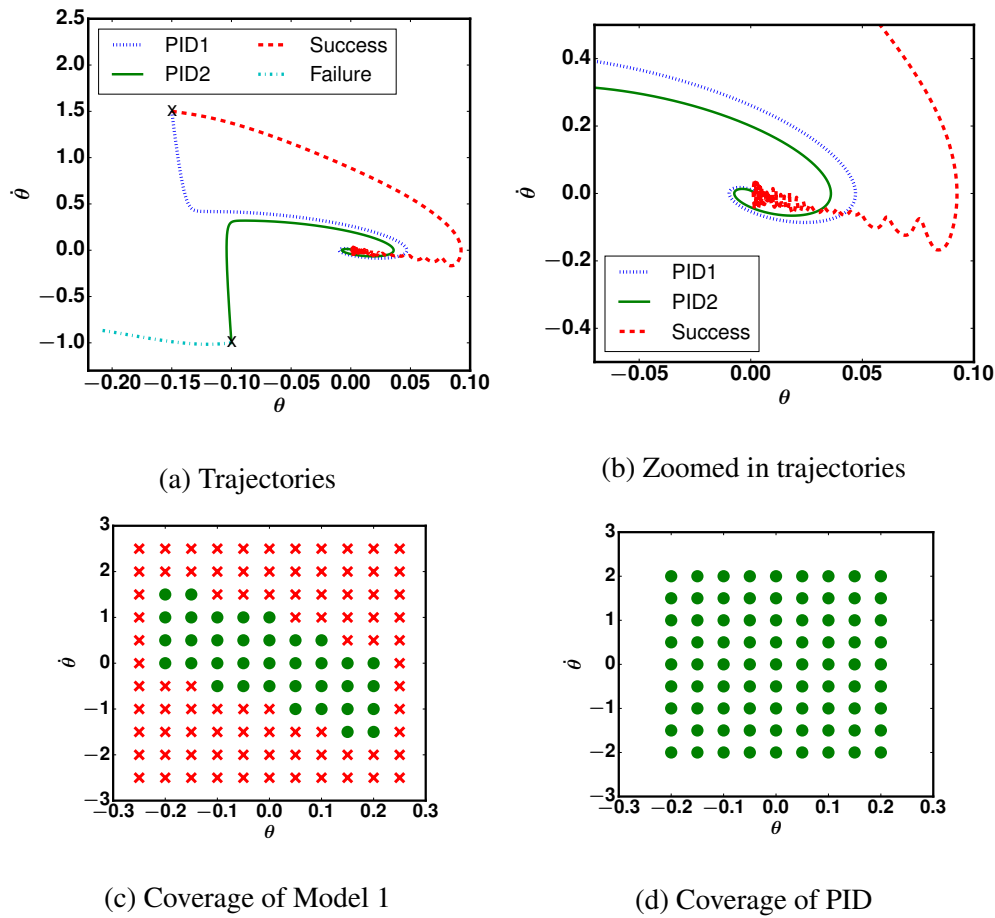


Figure 4: Trajectories and coverage of Model 1. (a) Trajectories of the plant state  $(\theta, \dot{\theta})$  for Model 1 after training and the PID controller, over time with different initial settings. The 'x' marks indicate the starting points and  $(0, 0)$  is the set point. There are two starting points,  $(-0.15, 1.5)$  where both the PID and Model 1 succeeded and  $(-0.1, -1.0)$  where the PID succeeded but Model 1 failed. (b) Trajectories in (a) zoomed in around the set point  $(0, 0)$  for improved visualization. The plant for Model 1 oscillates between  $(0, -0.02)$  and  $(0, 0.02)$  in the stable condition. (c) Coverage of initial states  $(\theta, \dot{\theta})$  for the Model 1 controller. That is, initial states that the controller succeeds in shepherding to the set point  $(0,0)$ . A green circle indicates a success while a red 'x' indicates a failure. (d) Coverage of the PID controller.

smaller than that of the PID's.

## 8.2 Model 2 (Multiple kernels Feedforward Network)

The next most complex controller is one where output neurons with different force kernels,  $\pm\kappa_1(t), \dots, \pm\kappa_N(t)$ , are trained to jointly accomplish the control task. We performed the learning experiments above for 4, 6, and 8 output neurons with successively larger force kernels. In this case, the force magnitude was assigned to the output neurons in a symmetric manner: equal magnitude kernels for left and right force were assigned to pairs of neurons. Extensive details of these learning experiments have been presented in [22]. Here we review the basic findings.

As in the case of Model 1, Model 2 controllers achieved the objective of stabilizing the plant and the spike trains exhibited regular patterns; neurons fired alternately periodically. In general, the spike train in the stable state was sparser than that in the start condition. We also observed that there were unnecessary spikes in the stable state. To elaborate, since there are neurons that generate large as well as small forces, one only needs the small force neurons to fire in the stable state. This behavior can be achieved by adding reciprocal synaptic communication between output neurons so that the neurons are aware of each other's spike trains, which leads us to the recurrent networks of Model 3 that we discuss in the next section.

As for the coverage of initial states that the controllers could stabilize, it increased with the number of neurons in the controller. When compared to the PID controller, Model 2's coverage was smaller, albeit larger than that of Model 1.

### 8.3 Model 3 (Multiple kernels Recurrent Network)

We performed the same set of learning experiments for Model 3 where the output neurons were now recurrently connected. Fig. 5 shows snapshots of the plant state and the spike trains of the controller with two output neurons, after training. The threshold for firing was set at 0.1 and the force magnitude was 500. Note that once the plant has been stabilized, it remains around the set point (0, 0) and the error function  $E$  also stays at around 0. When compared to Model 1, the spike trains were much sparser: the average firing rates of the two output neurons were 1.03Hz and 0.52Hz, respectively. In comparison, the firing rates for Model 1 were 33.94Hz and 34Hz. This was the outcome of the synapses between the output neurons having naturally converged during training to connection strengths such that when one neuron fired, the other stopped firing, as shown in Fig. 5a.

We also conducted experiments with 4, 6, and 8 recurrently connected output neuron controllers. Fig. 6 displays snapshots of their starting and stable conditions. The force magnitudes assigned to the 4 output neurons were -500, -10, 10, and 500. The average firing rate of the 4 output neurons combined was 13.18 Hz, shared between 6.6 Hz for the left neurons and 6.58 Hz for the right neurons. The firing rate per neuron was 3.3Hz. Fig. 6a shows that after training, the controllers stabilized the plant within a short period of time (1000 ms). Likewise, the average firing rate of the 6 output neurons controller was 13.05Hz (6.53, 6.52 Hz, for left and right neurons respectively), and the rate per neuron was 2.18Hz. For the 8 neuron controller, the average firing rate as shown in Fig. 6 (e) and (f) was 7.21Hz (3.14Hz left, 4.07Hz right) and the rate per neuron was 0.9Hz. Finally, Fig. 7 shows the coverage of initial states  $(\theta, \dot{\theta})$  that the Model 3 controllers

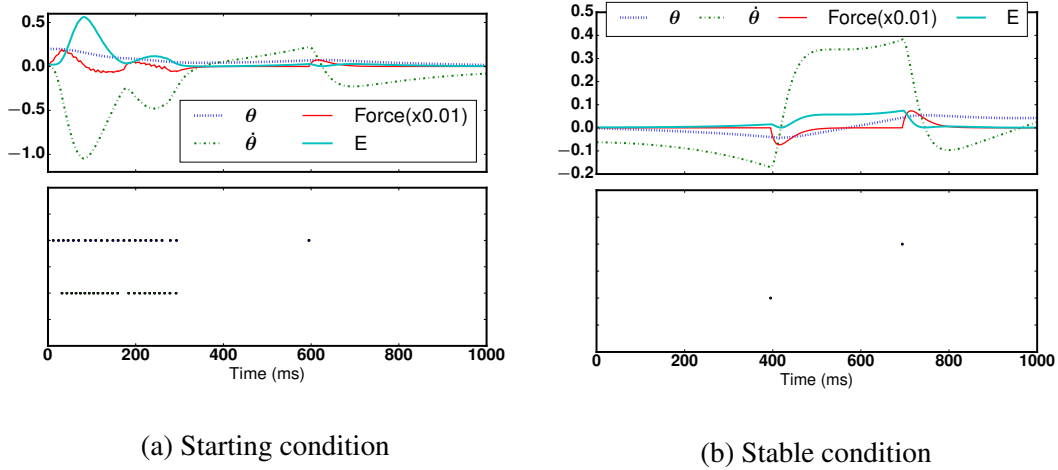
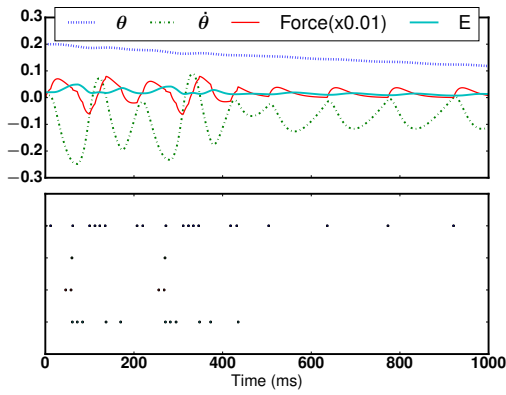
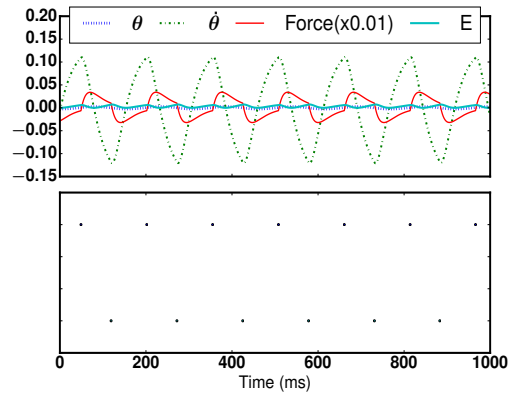


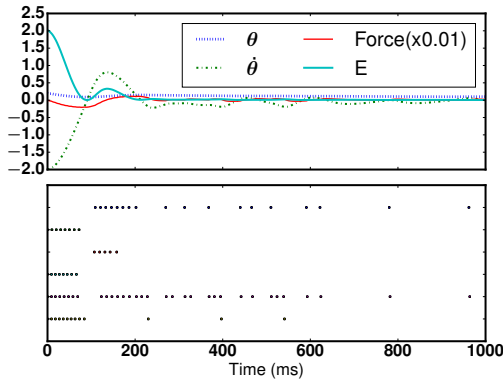
Figure 5: Snapshots of the plant state (top panels) and spike trains of the controller (bottom panels) for Model 3 with two output neurons, after training. In all the top panels, the blue dotted line is the vertical angle  $\theta$ , the green dash-dot is the angular velocity  $\dot{\theta}$ , the cyan solid line is the error function  $E$ , and the red solid line is the force applied to the plant. The final force applied to the plant is scaled down 100 fold ( $\times 0.01$ ) for improved visualization. (a) After training, the controller stabilizes the plant within a short period of time (1000 ms). The spike trains are sparse and exhibit patterns. (b) In the stable state, the pole oscillates around the set point (0, 0) and the error function  $E$  is also at around 0.



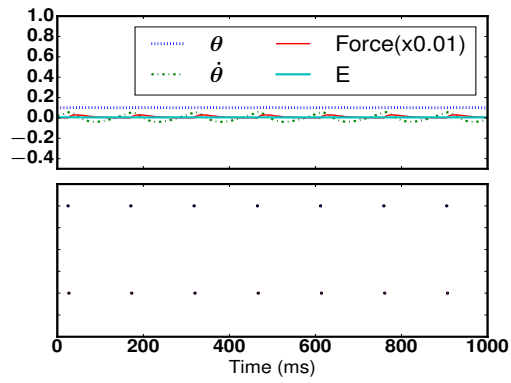
(a) Starting condition for 4 output neurons



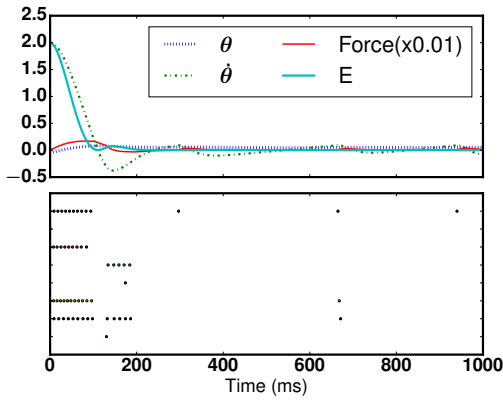
(b) Stable condition for 4 output neurons



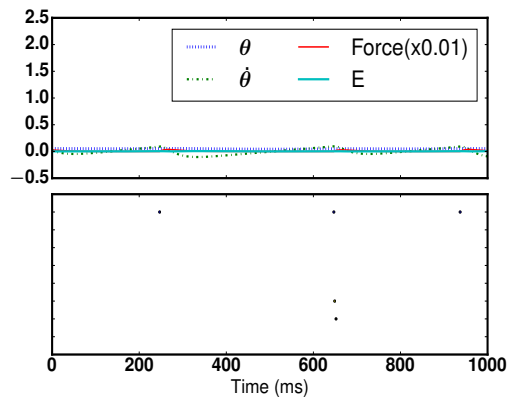
(c) Starting condition for 6 output neurons



(d) Stable condition for 6 output neurons



(e) Starting condition for 8 output neurons



(f) Stable condition for 8 output neurons

Figure 6: Snapshots of the plant state (top panels) and the spike trains of the controller (bottom panels) for Model 3 with recurrently connected 4, 6, and 8 output neurons, after training. The spike trains in all cases are sparse (0.9-3.3Hz per neuron).

with 2, 4, 6, and 8 output neurons managed to stabilize.

Interestingly, the reason why the spiking network controllers could not learn the corner cases was that there was very little time before the pendulum fell. The PID controller, not beholden to a learning process, does not suffer this problem. The very limited set of scenarios where the network controllers failed to learn is testament to the versatility of the learning process.

## 9 Experiments - Fish Locomotion

To further explore the capacity of the proposed controller, we considered the challenging task of locomotion. We used a fish plant with detailed emulation of musculature (the SOLEIL project [16]). The difficulty of this problem is apparent from the observation that unless the multiple controls, *yaw/pitch/roll* are operated synergistically, the task is impossible to achieve. Furthermore, vastly different control trajectories may be necessary for what would otherwise look like similar states, such as when the fish at the same location is oriented away from, instead of toward, the target. We used a simple routine mechanism to control the velocity of the fish and focused on the task of learning the *yaw/pitch/roll* controls. To elaborate, the velocity of the fish was set to a certain value, stay constant, and then ramp down to 0 when the target location fell within a threshold distance from the fish's center of gravity (*cog*).

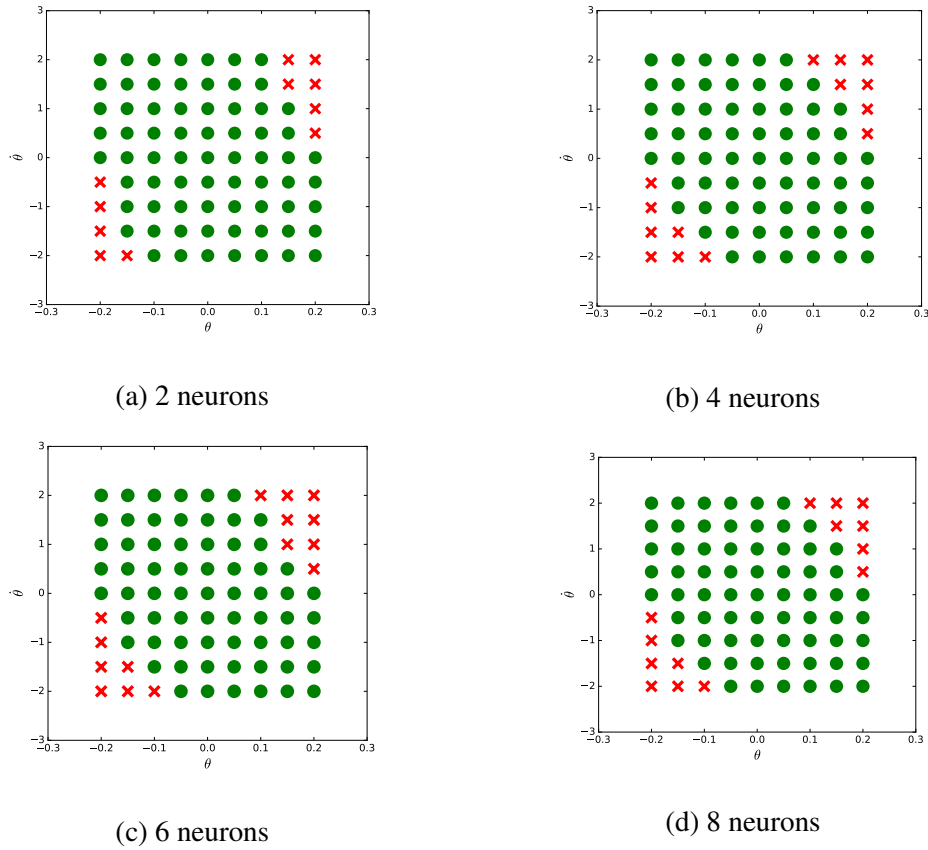


Figure 7: Stability coverages of initial plant states  $(\theta, \dot{\theta})$  for Model 3 with 2, 4, 6, and 8 output neurons, after training. A green circle indicates success while a red 'x' indicates failure for the corresponding initial state. (a) 2 output neurons covers 70 initial plant states among 81 attempted states (86.42%). This is larger than the 36 states (44.44%) achieved by Model 1. (b) 4 output neurons covers 67 states (82.72%). This is larger than the 45 states (55.56%) achieved by Model 2. (c) 6 output neurons covers 66 states (81.48%) compared to 51 (62.96%) of Model 2. (d) 8 output neurons covers 67 states (82.72%) compared to 62 (76.54%) of Model 2. Model 3 results are comparable to the PID controller which covers all 81 states (100%).

## 9.1 Setup

In all experiments, a fish was positioned in 3-dimensional space with initial location of its cog set as the origin  $(0, 0, 0)$ , and its head-to-tail axis oriented along the negative  $y$ -axis (facing negative  $y$ , with tail toward positive  $y$ ). The fish moved towards a target location  $(x^*, y^*, z^*)$  according to the velocity profile described in the previous section. The fish therefore stopped only when the controller had achieved its objective. The locomotion of the fish was controlled by a vector of  $\langle yaw, pitch, roll \rangle$  control forces as depicted in Figure 2b. The process variable input into the controller was the angle between the front to back axis of the fish and the fish centric vector pointing to the target location. We denote this angle vector process variable between the fish’s current orientation and the target by  $\langle \theta_x, \theta_y, \theta_z \rangle$ . In the learning experiments, the controller took as input the difference between the current angle vector  $\langle \theta_x, \theta_y, \theta_z \rangle$  and the desired angle vector  $\langle \theta_x^*, \theta_y^*, \theta_z^* \rangle$ , which was set at  $\langle 0, 0, 0 \rangle$ , and output a vector of  $\langle yaw, pitch, roll \rangle$  forces. The desired angle vector  $\langle 0, 0, 0 \rangle$  corresponded to the fish facing the target head on. The error function  $E$  was therefore  $\frac{1}{2} \sum_{i \in \{x, y, z\}} (\theta_i^* - \theta_i)^2$ . For the simulations, we defined a successful learning event as one where the fish reached the target location. Formally, a success is defined as an event where the Euclidean distance  $D$  between the fish and the target is within a certain predefined threshold. We conducted two sets of experiments, one where the fish was constrained on a 2-dimensional plane containing the target (all locations here being  $(x, y, 0)$ ) and one where the fish moved in the full 3-dimensional space. We set the threshold  $D$  at 0.06 for the 2-dimensional experiments and 0.1 for the 3-dimensional experiments. With this setup, training of the controller was continued until a success. In the training phase, the controller started with random

network weights and a randomly chosen target location; the fish started at the origin  $(0, 0, 0)$ . The controller then learned to control the locomotion of the fish by updating the synaptic weights. Unless stated otherwise, the training method and configurations of the controllers were the same as those of the inverted pendulum. We note in passing that there is an upper limit to the force magnitude that can be applied to the plant. When the force magnitude crosses this bound, the fish moves unrealistically. Unless otherwise stated, the force magnitude assigned to any output neuron was 50.

## 9.2 Results

We present experimental results in the 2-dimensional case for two controller network architectures, feedforward followed by recurrent.

### 9.1 Model 1 (Feedforward Network)

We first used a feedforward network of neurons to learn the control task when the fish was restricted to a 2-dimensional plane containing the target location. Note that the task was, in theory, achievable with the control of just the *yaw*, and therefore we considered a Model 1 network with two neurons forcing yaw left or right. The network learned the task with ease. Fig. 8 shows snapshots of the system state and spike trains of the controller for Model 1 with 2 output neurons, after training.

Observe that when the fish gets close to the destination in terms of angular alignment, the neurons stop generating spikes. The dense spike trains in the bottom panel are due to the practical limits on the force magnitude that can be applied to the plant at one time, as mentioned earlier. If this force is too large, the fish spins around unreal-

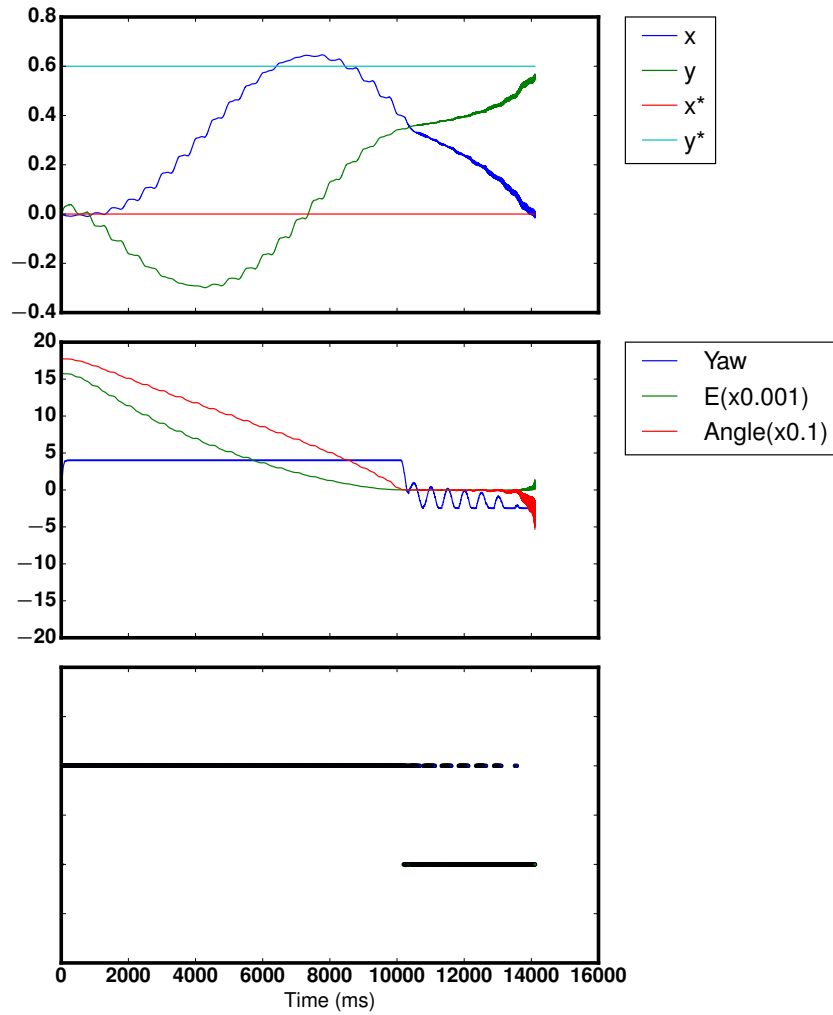


Figure 8: Snapshot of the system state and spike trains of the controller for Model 1 with 2 output neurons after training. The control variable  $\langle yaw \rangle$  was controlled. The target location  $(x^*, y^*, z^*)$  is  $(0, 0.6, 0)$ . In the top panel, the blue dotted line is the  $x$ -coordinate of the fish's cog, the green dash-dot is the  $y$ -coordinate, and the red solid line is the  $z$ -coordinate. In the middle panel, shown are the error function  $E$ , the distance  $D$  between the fish and the target, and the  $\langle yaw \rangle$  force applied to the fish, respectively. In the bottom panel, the spike trains of the output neurons corresponding to  $\langle +yaw, -yaw \rangle$  forces are displayed.

istically. Since the network is not allowed to generate a large force at once, in contrast to the case of the inverted pendulum controller, the neurons generate multiple spikes to compensate.

## 9.2 Model 3 (Recurrent Network)

We repeated the 2-dimensional experiments with a recurrent network of two output neurons trained to achieve the same control task. Training was successful here as well. Fig. 9 shows snapshot of the system state and spike trains of the controller for Model 3 with 2 output neurons, after training.

Fig. 10 compares the coverages of target locations,  $(x^*, y^*, 0)$  for Model 1 and Model 3 controllers with two output neurons. Coverage is defined as the set of target locations that the trained controller could shepherd the fish to. Note that the initial orientation of the fish with respect to the target location plays a big role in whether a target is achievable, particularly when the target is very close.

# 10 Conclusion

We have proposed spiking neuron network controllers that are biologically plausible and have applied them to learn the classical cart-pole control problem as well as a fish locomotion control problem, to demonstrate their efficacy. The derivation of the synaptic update rule is general and can be applied to any feedforward or recurrent network of spiking neurons. The experiments show that the proposed controllers have fairly large regions of stability, and behave in a manner different from traditional PID controllers. We have analyzed in detail multiple network architectures with different output neu-

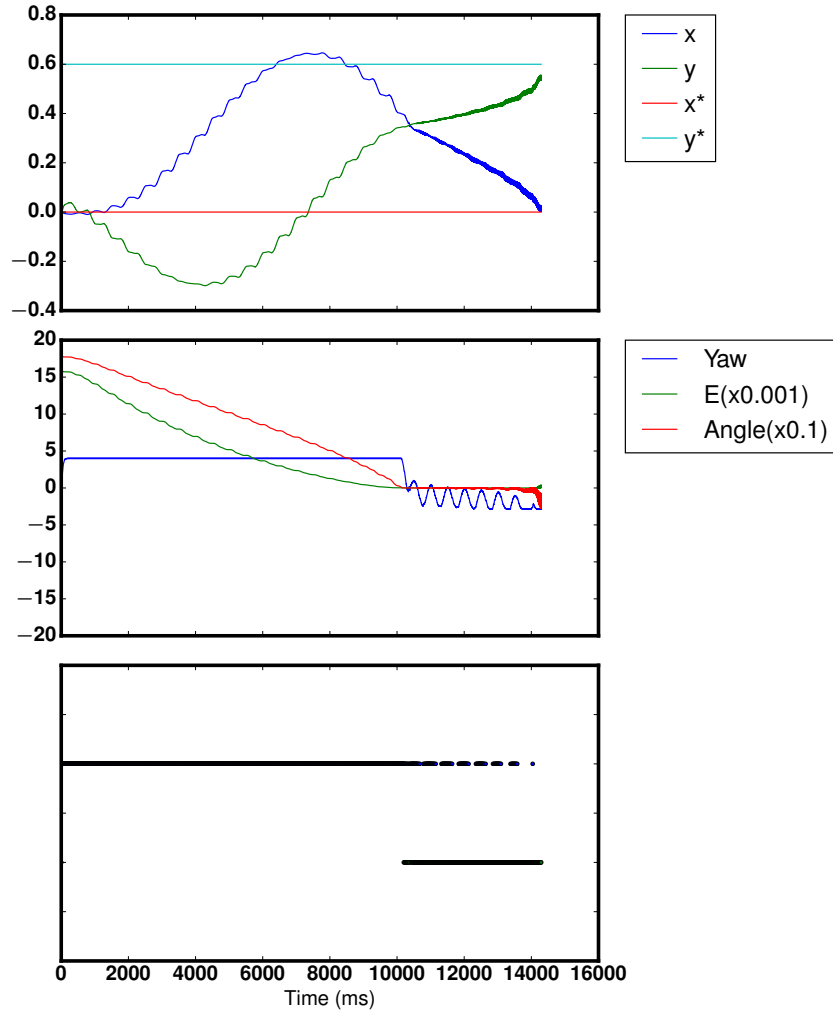
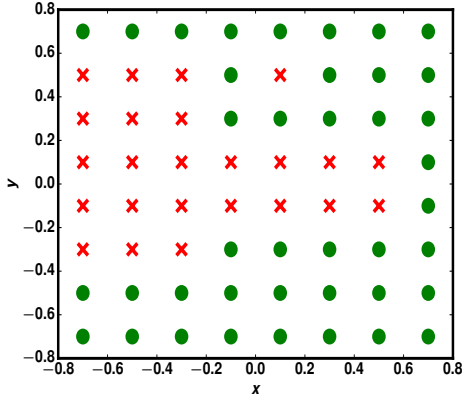
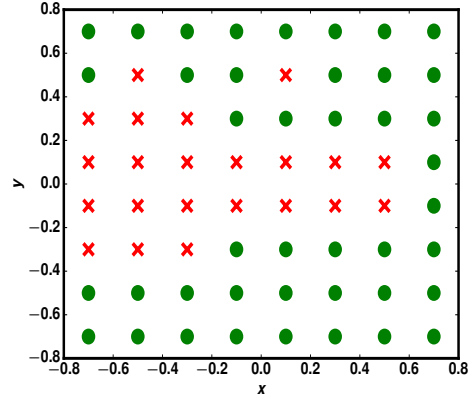


Figure 9: Snapshot of the system state and spike trains of the controller for Model 3 with 2 output neurons after training. The control variable  $yaw$  was controlled. Note that the results are almost identical to that of the feedforward network with 2 neurons. The target location  $(x^*, y^*, z^*)$  is  $(0, 0.6, 0)$ . In the top panel, the blue line is the  $x$ -coordinate of the fish's cog, the green line is the  $y$ -coordinate, and the red line is the  $z$ -coordinate. In the middle panel, shown are the error function  $E$ , the distance  $D$  between the fish and the target, and the  $\langle yaw \rangle$  force applied to the fish, respectively. In the bottom panel, the spike trains of the output neurons corresponding to  $\langle +yaw, -yaw \rangle$  forces are displayed.



(a) Coverage for Model 1



(b) Coverage for Model 3

Figure 10: Coverages of the target location  $(x^*, y^*, 0)$  for Models 1 and 3 with two output neurons, after training. A green circle indicates a success while a red 'x' indicates a failure for the corresponding target location. (a) Model 1 with two output neurons. (b) Model 3 with two output neurons. Both models have a similar range of coverage although Model 3 has a slightly larger region (65.63%) than Model 1 does (62.50%).

ron settings: two output neurons with the same force magnitude (Model 1), 4 or more neurons with different force magnitude kernels (Model 2), and recurrently connected neurons with multiple force kernels (Model 3). From the experiments, we deduce that more neurons with diverse force magnitudes can learn larger coverage domains and are thus more flexible and robust. Furthermore, we showed that the recurrent network controllers can produce very sparse spike train outputs with firing rates as low as 0.9 Hz per neuron signifying high energy efficiency. Finally, we have demonstrated that the controller can learn even in a scenario where several control variables have to be regulated synergistically to accomplish the control task.

Future directions that we wish to consider are: adding kernels for filtering the process variable inputs, and more general control cost functions. The former can readily

be added to the current framework keeping the derivation the same. The latter requires using more general error functions and analyzing their impact on the resultant control behavior.

## Acknowledgments

The authors thank the Air Force Office of Scientific Research (Grant FA9550-16-1-0135) for their generous support of this research.

## References

- [1] Anderson, C. W. (1987). Strategy learning with multilayer connectionist representations. In *Proceedings of the Fourth International Workshop on Machine Learning*, (pp. 103–114).
- [2] Anderson, C. W. (1988). Code for learning to balance a pole. <http://www.cs.colostate.edu/~anderson/code/poledemo.tar.gz>.
- [3] Banerjee, A. (2006). On the sensitive dependence on initial conditions of the dynamics of networks of spiking neurons. *Journal of computational neuroscience*, 20(3), 321–348.
- [4] Banerjee, A. (2016). Learning precise spike train-to-spike train transformations in multilayer feedforward neuronal networks. *Neural Comput.*, 28(5), 826–848.
- [5] Barto, A. G., Sutton, R. S., & Anderson, C. W. (1983). Neuronlike adaptive

- elements that can solve difficult learning control problems. *Systems, Man and Cybernetics, IEEE Transactions on, Sep(5)*, 834–846.
- [6] Batllori, R., Laramée, C. B., Land, W., & Schaffer, J. D. (2011). Evolving spiking neural networks for robot control. *Procedia Computer Science*, 6, 329–334.
- [7] Bohte, S. M., Kok, J. N., & La Poutre, H. (2002). Error-backpropagation in temporally encoded networks of spiking neurons. *Neurocomputing*, 48(1), 17–37.
- [8] Bouganis, A., & Shanahan, M. (2010). Training a spiking neural network to control a 4-dof robotic arm based on spike timing-dependent plasticity. In *Neural Networks (IJCNN), The 2010 International Joint Conference on*, (pp. 1–8). IEEE.
- [9] d’Avella, A., & Bizzi, E. (2005). Shared and specific muscle synergies in natural motor behaviors. *Proceedings of the National Academy of Sciences of the United States of America*, 102(8), 3076–3081.
- [10] d’Avella, A., Portone, A., Fernandez, L., & Lacquaniti, F. (2006). Control of fast-reaching movements by muscle synergy combinations. *Journal of Neuroscience*, 26(30), 7791–7810.
- [11] Flash, T., & Hogan, N. (1985). The coordination of arm movements: an experimentally confirmed mathematical model. *Journal of neuroscience*, 5(7), 1688–1703.
- [12] Floreano, D., & Mattiussi, C. (2001). Evolution of spiking neural controllers for autonomous vision-based robots. *Evolutionary Robotics. From Intelligent Robotics to Artificial Life*, (pp. 38–61).

- [13] Florian, R. V. (2012). The chronotron: a neuron that learns to fire temporally precise spike patterns. *PLoS one*, 7(8), e40233.
- [14] Francis, B. A., & Wonham, W. M. (1976). The internal model principle of control theory. *Automatica*, 12(5), 457–465.
- [15] Frémaux, N., Sprekeler, H., & Gerstner, W. (2013). Reinforcement learning using a continuous time actor-critic framework with spiking neurons. *PLoS computational biology*, 9(4), e1003024.
- [16] Fuentes, M., Pinon, B., & Munnier, A. (2012). The SOLEIL project: Fish locomotion. <http://soleil.gforge.inria.fr/>.
- [17] Gerstner, W., & Kistler, W. M. (2002). *Spiking neuron models: Single neurons, populations, plasticity*. Cambridge university press.
- [18] Gütig, R., & Sompolinsky, H. (2006). The tempotron: a neuron that learns spike timing-based decisions. *Nature Neuroscience*, 9(5), 420–8.
- [19] Hagaras, H., Pounds-Cornish, A., Colley, M., Callaghan, V., & Clarke, G. (2004). Evolving spiking neural network controllers for autonomous robots. In *Robotics and Automation, 2004. Proceedings. ICRA'04. 2004 IEEE International Conference on*, vol. 5, (pp. 4620–4626). IEEE.
- [20] Hennequin, G., Vogels, T. P., & Gerstner, W. (2014). Optimal control of transient dynamics in balanced networks supports generation of complex movements. *Neuron*, 82(6), 1394–1406.

- [21] Hoff, B., & Arbib, M. A. (1993). Models of trajectory formation and temporal interaction of reach and grasp. *Journal of motor behavior*, 25(3), 175–192.
- [22] Kang, T. S., & Banerjee, A. (2017). Learning deterministic spiking neuron feedback controllers. In *Neural Networks (IJCNN), 2017 International Joint Conference on*, (pp. 2443–2450). IEEE.
- [23] Memmesheimer, R.-M., Rubin, R., Ölveczky, B. P., & Sompolinsky, H. (2014). Learning precisely timed spikes. *Neuron*, 82(4), 925–938.
- [24] Moheemmed, A., Schliebs, S., Matsuda, S., & Kasabov, N. (2012). Span: Spike pattern association neuron for learning spatio-temporal spike patterns. *International Journal of Neural Systems*, 22(04), 1250012.
- [25] Song, S., Miller, K. D., & Abbott, L. F. (2000). Competitive hebbian learning through spike-timing-dependent synaptic plasticity. *Nature neuroscience*, 3(9), 919–926.
- [26] Squire, L., Berg, D., Bloom, F. E., Du Lac, S., Ghosh, A., & Spitzer, N. C. (2012). *Fundamental neuroscience*. Academic Press.
- [27] Takase, N., Botzheim, J., & Kubota, N. (2015). Evolving spiking neural network for robot locomotion generation. In *Evolutionary Computation (CEC), 2015 IEEE Congress on*, (pp. 558–565).
- [28] Ting, L. H., & Macpherson, J. M. (2005). A limited set of muscle synergies for force control during a postural task. *Journal of neurophysiology*, 93(1), 609–613.

- [29] Todorov, E., & Jordan, M. I. (2002). Optimal feedback control as a theory of motor coordination. *Nature neuroscience*, 5(11), 1226.
- [30] Tresch, M. C., Saltiel, P., & Bizzi, E. (1999). The construction of movement by the spinal cord. *Nature neuroscience*, 2(2).
- [31] Uno, Y., Kawato, M., & Suzuki, R. (1989). Formation and control of optimal trajectory in human multijoint arm movement. *Biological cybernetics*, 61(2), 89–101.
- [32] Wiklendt, L. (2014). *Spiking neural networks for robot locomotion control*. PhD thesis, University of Newcastle. Faculty of Engineering & Built Environment, School of Electrical Engineering and Computer Science.
- [33] Zajac, F. (1989). Muscle and tendon: properties, models, scaling, and application to biomechanics and motor control. *Critical reviews in biomedical engineering*, 17(4), 359.